J Mater Sci (2018) 53:15142–15156

Composites

Effect of surfactants on the properties of a gas-sealing coating modified with fly ash and cement

Huiping Song[1,2], Wensheng Xie[1], Jianqiang Liu[1], Fangqin Cheng[1,*], Khaled A. M. Gasem[2], and Maohong Fan[2]

[1] *Institute of Resources and Environmental Engineering, Collaborative Innovation Center of High Value-added Utilization of Coal-related Wastes, Shanxi University, No. 92, Wucheng Road, Taiyuan 030006, Shanxi, China*

[2] *Departments of Chemical and Petroleum Engineering, University of Wyoming, Laramie, WY 82070, USA*

Received: 18 April 2018
Accepted: 10 July 2018
Published online: 2 August 2018

ABSTRACT

Gas leakage seriously threatens the safety of workers in coal mines. Spraying the gas-sealing coating is one of the effective methods to relieve gas leakage. However, the hydrophobic property of coal makes it difficult for the gas-sealing coating to penetrate the coal. The effect of surfactants on the properties of the hybrid organic–inorganic, gas-sealing coating was systematically studied. Analysis of the influence of different surfactants on the contact angle of coating and coal shows that the contact angle reduction of tributyl phosphate (TBP) is unaffected by the emulsion concentration. The reduction is more than 30%, which effectively improves the wettability of the coal surface. Further, TBP addition can optimize the micro-morphology, internal microstructure, and bonding strength. TBP addition can also facilitate a close contact on the interface, thus achieving effective penetration within the coal sample and enhancing the gas-sealing performance of the coating. In addition, this study explores preliminarily the curing mechanism and synthetic model of the coating, providing a new theoretical basis for the development of gas-sealing coatings.

Introduction

Coal is currently an essential element of China's energy portfolio. To promote safe coal production, an effective method for sealing underground coal mines is a top safety priority [1, 2]. In recent years, China has made great efforts to develop effective gas-sealing materials in coal mines [3]. The research on the gas-sealing material is mainly focused on the basic material ratio, mechanics, and airtight performance. No detailed research has been conducted on actual material application [4, 5]. Coal has strong hydrophobic property. As such, when the sealing material is sprayed on the coal wall, the hydrophobic property of coal will impede the penetration of sprayed material into coal [6]. The relatively complex application environment in underground coal mines also exerts important influence on the actual application of the gas-sealing materials [7]. In this regard, improving the chemical properties of the coating and

Address correspondence to E-mail: cfangqin@sxu.edu.cn; chenghg1978@126.com

https://doi.org/10.1007/s10853-018-2679-4

coal wall surface and making the coating penetrate well into the coal wall and closely bond with it is of great importance in improving the comprehensive gas-sealing performance in actual material applications.

Some functional additives are often added for coating preparation. These additives are mainly used for inhibiting the production of bubbles during coating production and optimizing the micro-pore structure inside the coating or adjusting the coating property [8]. The wettability of coal and the coating liquid usually depends on their surface tension and contact angle, whose measurement has also been widely used in the evaluating the wetting behaviour on the coal surface. In this regard, studies have shown that adding sodium dodecyl sulphate in deionized water can significantly improve the wetting behaviour of coal [9]. Adding sodium dodecyl benzene sulphonate in water for a multicomponent combination and then spraying the mixture on the coal particles can reduce the contact angle with the coal and slow down the emission of gas from coal pores [10]. Therefore, adding appropriate surfactant in the gas-sealing coating is expected to be an effective way to improve the wettability of materials on the coal surface, which is worthy of further study.

In general, many different surfactants exist, including silicone oil-based defoamer, mineral oil-based defoamer and phosphate-based defoamer. Defoamers based on silicone are more effective, but they are too expensive [11] and they do give rise to the 'much dreaded silicone oil spots' [12], so they are not suitable to the gas-sealing coating in coal mines. The efficiency of non-silicone defoamers (mineral oil- and phosphate-based defoamers) are lower than that of silicone defoamers; however, they are significantly inexpensive as compared to silicone-based defoamers; therefore, they are commonly used in the middle-grade or low-grade coatings. As such, considering the requirements for wettability, dispersion, stability, and other performance metrics as well as safety, efficiency, and economy, three surfactants suitable for water-borne styrene-acrylic emulsion system were selected in this study. They were the phosphate-based defoamer TBP and two mineral oil-based defoamers SD202 and F202, respectively.

In this study, the hybrid organic–inorganic gas-sealing coating prepared with ultrafine fly ash (UFA) and cement in previous research [13] was used as the basic coating formula. The suitable surfactant concentrations were determined based on the most wettability between the coating and the coal wall. For the purpose, the effect of different surfactants on the surface tensions and contact angles between the emulsion of series concentrations and the coal wall was investigated. The micro-permeability of the gas-sealing material and the pore structure were also analysed. In addition, this study proposed a curing mechanism and a synthesis model, which will provide a theoretical foundation for the actual application of the gas-sealing coating.

Materials and methods

Materials

The main materials were styrene-acrylic emulsion S400F (Basf Company), UFA (Shanxi Huatong Company) and Portland cement (325#, Taiyuan Cement Company). Their particle sizes were measured by the Particle Size Analyser (Eyetech/CIS, Ankersmid B.V., Holland). Their average sizes were around 0.2 μm, 2.2 μm and 18.1 μm, respectively. Aluminium hydroxide (analytical reagent, Tianjin Guangfu), Antimonous oxide (Sb_2O_3, analytical reagent, Tianjin Guangfu), 70# chlorinated paraffin (analytical reagent, Tianjin Guangfu), zinc borate (analytical reagent, Tianjin Guangfu), graphite (analytical reagent, Tianjin Guangfu), conductive carbon black (analytical reagent, Tianjin Guangfu). Surfactants include two mineral oil-based defoamers, SD202 (Industrial-grade, Shanghai Wenhua) and F202 (Industrial-grade, Zhejiang Linan), and one phosphate-based defoamer TBP (Analytical reagent, Tianjin Hengxing).

Experimental method

Method for measuring the surface tension

The surface tension of the solution was measured with the surface tension meter (QBZY, Fangrui, Shanghai) using the plate insertion method. The emulsion–water mixture solution with the emulsion concentration of 0.1 g L^{-1} was prepared at 20 °C. Its surface tension was measured to be 72.92 mN m^{-1}. Then, different surfactants were added in the mother solution and mixed evenly to prepare a series of solutions. The solutions were moved to the energy-

saving intelligent thermostatic bath (DC-2006, Xinzhi, Zhejiang) at 20 °C for testing.

Method for measuring the contact angle

Large coal was cut, ground, and sanded to obtain relatively horizontal coal samples with smooth upper and lower surfaces. Surfactants were added to prepare different solutions for testing. The contact angles between the droplets and the coal surface were determined at room temperature with the contact angle meter (JC2000X6, Zhongchen, Shanghai) using the hanging drop method [14, 15]. The contact angle between the flow interface and the solid interface at the junction of three phases was automatically measured by the tangent method on the droplet images, which was also the contact angle between the droplet and the coal.

Method for preparing and testing of coating

The preparing procedures of coating in this study were outlined in previous research. Water was added to the styrene-acrylic emulsion. After well-mixed with a glass rod, the emulsion was mixed in a disperser (KS-370, Shanghai) for 1 min. Subsequently, solid powder that was already well-mixed was added and mixed up by a glass rod. The viscosity of mixture was monitored by a digital viscometer (STM-IVB, Shanghai) and was maintained about 80KU by adding water, and then the admixture was stirred by disperser at 600r/min for 5 min. After sitting for 2 min, the mixed coating materials were poured into a template, ageing for 7 days and ready for using [13].

The bonding strength was measured by a SW-6000C bond strength tester with high precision (Beijing Shengshi).

A gas permeation meter (VAC-V1, Languang, Ji'nan) was used to determine the air permeation of these coating samples. The air permeation testing method was in reference to the national standard Determination for Gases Permeability of Vulcanized Rubber or Thermoplastic (GB/T7755-2003). Meanwhile, the appearance of samples was observed and elemental analysis was investigated by SEM–EDS (Tabletop Microscope TM3030, Hitachi, Japan).

Results and discussion

Critical micelle concentration (CMC) of different surfactants

The surface tensions of the surfactants of different concentrations in the emulsion-water solution at the emulsion concentration of 0.1 g L^{-1} were measured to obtain the concentration value of the surfactants with the maximum reduction of the contact angle between the coating and the coal wall. The results shown in Fig. 1 indicate that the surface tension of the solution is reduced after adding the surfactant. However, when the surfactant concentration increases beyond a certain level, an obvious turning point is observed. At this concentration, which is called the critical micelle concentration (CMC), the solution begins to form micelles [16]. The CMC is determined by the intersection of two straight lines on the relation graph between the concentration and the surface tension [17]. After measurement, the CMC value was 0.08% for TBP, 0.02% for F202, and 0.16% for SD202.

Contact angle of coal

Usually, the contact angle value is used to represent the wettability of the liquid to the solid. Small contact angle means good wettability of the liquid to the solid surface. The wetting contact angle between coal and water is generally 60° to 85° [18]. Coal is a kind of substance with strong hydrophobic property. Therefore, adding appropriate surfactants in the liquid to

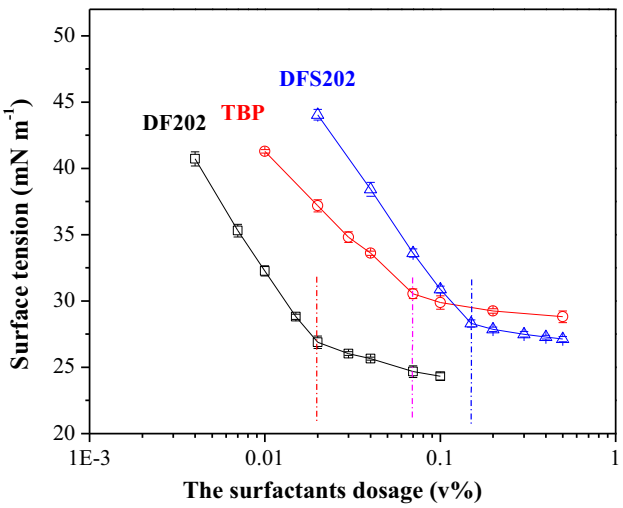

Figure 1 Effect of different surfactants and different adding amounts on the surface tension of the solution.

modify its behaviour, and thus improve the wettability of the coal and enhance the adhesive ability between the coating and the coal, is feasible. By testing, the stable contact angle between coal and water was 65°, indicating that the coal showed typical wettability and can be used to carry out the follow-up experimental research.

To investigate the effect of this modification and adaptability of the surfactant on the coating, a comparison was performed on the contact angles between the solutions and the coal after adding TBP, F202, and SD202 and those without surfactant addition. The dynamic contact angle values within 2 min were recorded by continuous photography method, as shown in Fig. 2. In the figure, the emulsion concentration of 1.7 g mL^{-1} represents the real proportion for coating preparation, and 2.9 g mL^{-1} is the maximum proportion which may be selected in actual operations in the future.

Figure 2 shows that the contact angles between the solutions of different concentration and the coal change significantly within 20 s and then become stable after 60 s. For the solutions without the surfactant in Fig. 2a, the initial contact angles between the solution and the coal increased with the increase in the emulsion concentration. However, when the contacting time was longer than 1 min, the contact angles between different solutions and the coal all maintained 60° angle and became stable. This phenomenon indicated that wetting and penetration of the coal surface were difficult for the solutions of different emulsion concentrations, which affected the gas-sealing effect of the coating on the coal wall during application to some extent. Therefore, the

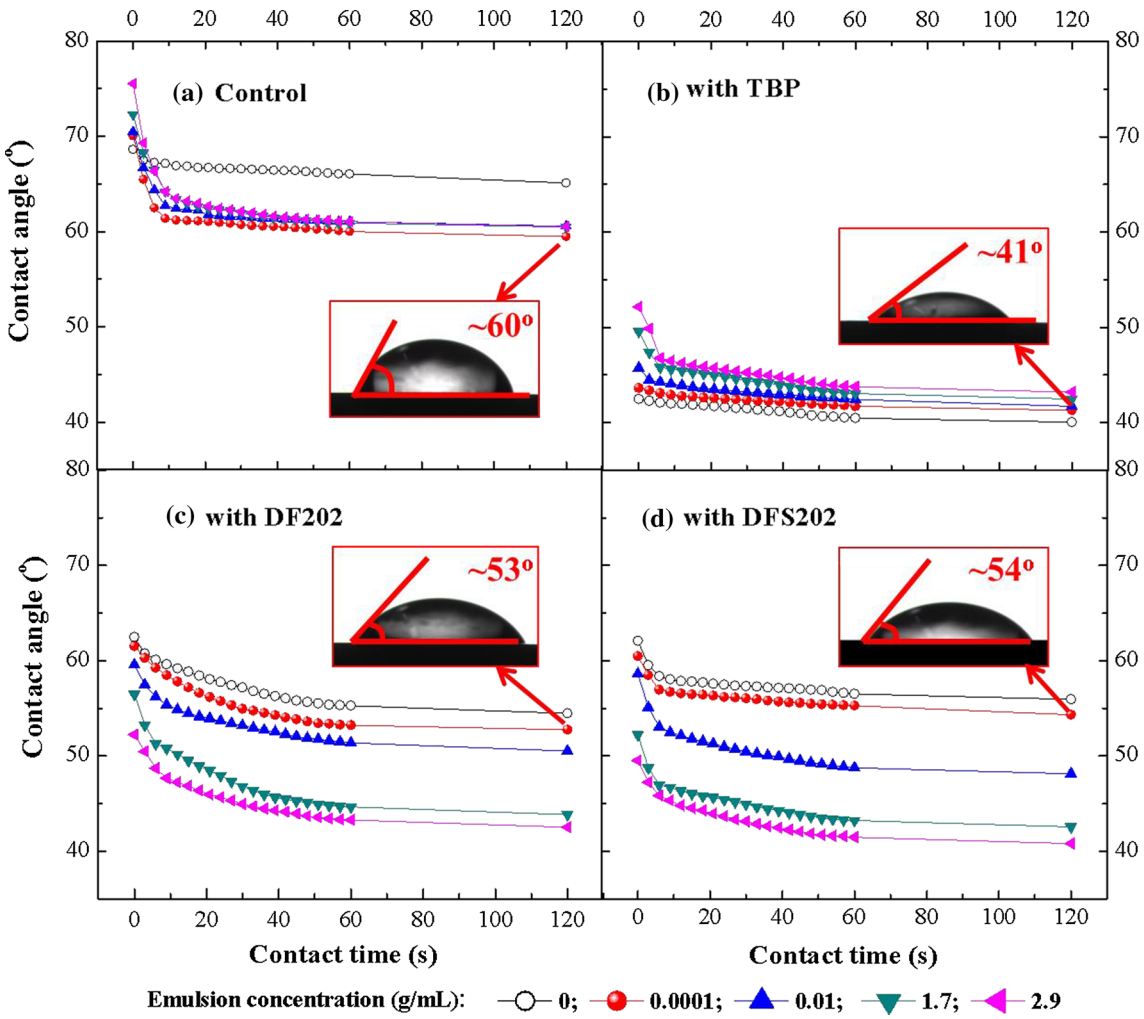

Figure 2 Change of the contact angles between the coatings of different emulsion concentrations and the coal over time.

material wettability on the coal wall must be improved.

The reduction amplitudes of different surfactants on the contact angle between the solution and the coal can be calculated by Eq. (1), and the results are shown in Fig. 3.

$$\Delta Q = (Q_{\text{initial}} - Q_{\text{TBP}})/Q_{\text{initial}} \times 100\% \quad (1)$$

Here, ΔQ is the reduction amplitude of contact angle; Q_{initial} is the contact angle of initial emulsion-water solution to coal; Q_{TBP} is the contact angle of solution with TBP.

Figures 2b and 3 show that the reduction performance of TBP was not affected by the emulsion concentration of the solution. TBP not only reduced the initial contact angles between the materials of different emulsion concentrations and the coal wall significantly but also kept the contact angles at 40°–42.5° after stability in Fig. 2b. The reduction amplitude of contact angle was up to 30–40%, reflecting the good wetting effect on the coal surface. This result indicates that TBP exhibits good adaptability in actual application. From the comparison of the contact angles (red dot and red line) in Fig. 2a, b, the contact angle was reduced from 60° to approximately 41° by TBP addition. TBP is poorly soluble in water; the TBP solubility at 20° in the pure water was approximately 0.095% [19]. In this study, when the added TBP concentration was 0.08%, TBP is fully mixed in the solution. Thus, when TBP was added, the contact angles between different materials and the coal wall after stability were not affected by the emulsion concentration, and they can all be kept at a low range.

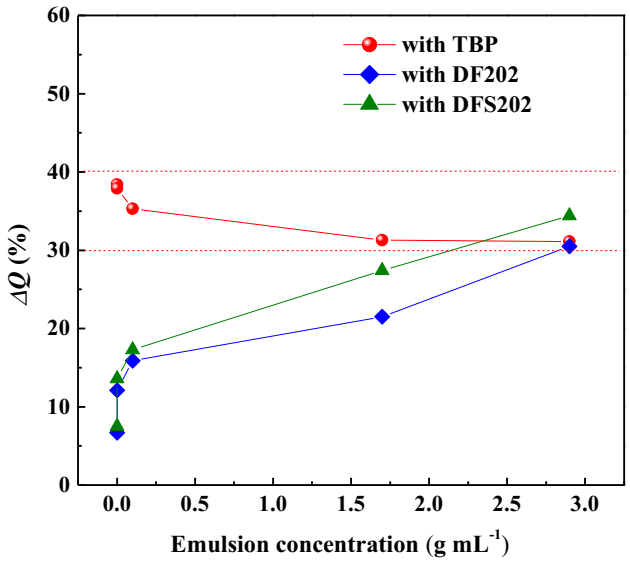

Figure 3 Reduction amplitude of different surfactants on the contact angles between the coatings of different emulsion concentrations and the coal.

According to Figs. 2c, d and 3, after adding F202 and SD202, the reduction amplitude in the contact angle between the coating and the coal was greatly affected by the emulsion concentration. Those two materials showed a consistent trend for the reduction effect of the contact angles with different emulsion concentrations. When the emulsion concentration was low, they both exhibited no obvious reduction in the initial contact angles and those after stability. With the rise in the emulsion concentration, both initial contact angles began to reduce, and the reduction amplitudes increased. This phenomenon may be occurring because F202 and SD202 are mainly composed of hydrophobic components and aliphatic mineral oil, which are extremely difficult to dissolve in water but exhibit good solubility in the styrene acrylic emulsion. Meanwhile, low emulsion concentration is not conducive to the dissolution and dispersion of F202 and SD202. With the rise in the emulsion concentration, their solubility in the mixed solution is greatly increased, thus changing the material wettability on the coal wall.

Effect of TBP on bonding strength of coating

According to the apparent property, water adsorption ratio, mechanical property, flame retardation and antistatic properties, the basic formula for gas-sealing coating (50 g emulsion, 60 g UFA, 20 g cement, 5 g chlorcosane, 3 g aluminium hydroxide, 4 g zinc borate, 3 g antimonous oxide, 3 g graphite, 2 g conductive black and 29 ml water) was given in the previous research [13]. This work studies the effect of TBP based on this coating formula. The bonding strength of the samples at 7 days with and without TBP is shown in Fig. 4. The bonding strength of the coating samples with TBP was all larger than that without TBP. TBP addition can significantly improve the wettability of the coatings on the surface of the substrate and promote the materials to penetrate the substrate effectively. Thus, the bonding strength of the coatings improved significantly.

Meanwhile, increasing the amount of added UFA from 0 to 60% increases the growth rates of the strength to 32.5%. When the added UFA amount was

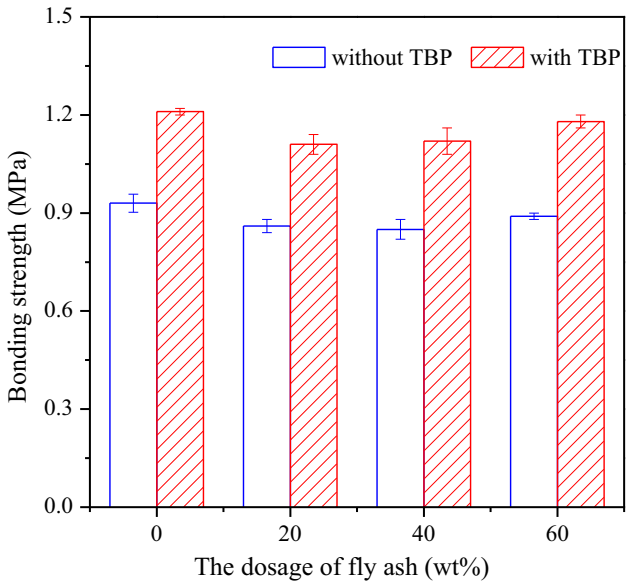

Figure 4 The bonding strength of the coatings without TBP and with TBP (curing 7d).

60%, the bonding strength after 7 days of curing was close to that of complete cement. This finding may be because the even distribution of UFA and ordinary cement promoted good gradation in the coating. Further, TBP addition can improve the liquidity and wettability of the coating and promote the pozzolanic UFA reaction inside the coating. The dual function of TBP promoted the bonding strength of the coating and improved it significantly.

The bonding strength of the coating aged for 14 days will be higher than that of all cement coating [13]. However, given that fast curing is expected in actual applications, the study simply compares the curing effect after 7 days. In addition, UFA addition can reduce the sealing cost with projections of good quality. Thus, the formula of 60% UFA at 7 days of curing will be selected.

Effect of TBP on the air tightness of coating and the microscopic analysis

Effect of TBP on the air tightness of coating

Tests and analyses were conducted on the effect of TBP on the air tightness of full-cement coatings and those containing 60% UFA. According to Table 1, TBP significantly improved the air tightness of the coatings. This outcome was mainly because TBP eliminated the bubbles created during coating preparation, avoided the formation of large holes, and improved the liquidity of various powder particles in the coatings. This condition results in uniform and dense internal structure of the coatings after curing and thus improving the air tightness of the coatings. It has been reported [20] that the material possesses good air tightness when the permeability coefficient is in the order of magnitude 10^{-10}. The permeability coefficient of 60% UFA samples with TBP was 1.84×10^{-10} cm^3 cm m^{-2} s^{-1} $cmHg^{-1}$. When this coating is sprayed on the wall of underground coal mine, it could effectively prevent the leakage of gas by increasing the mass transfer resistance.

Effect of TBP on the coating microstructure

The pore structure of materials is a direct factor in affecting their airtight performance. Good pore structure is critical to the gas-sealing performance of the materials [20]. Scanning electron microscopy (SEM) was used to conduct the analysis on the surface and inner microstructure of the coatings containing 60% UFA with and without TBP to explore the effect of TBP on the microstructure of the coatings and explain its influence on the air tightness of the coatings.

Surface microstructures in Fig. 5 show that the surface of the sample without TBP was very uneven. During curing, several shrinkage cavities were formed because of bubble bursting. No obvious shrinkage cavity was observed on the surface of the sample with TBP. The surface of the sample was flat with only a small number of fine lines on it after curing. This finding indicated that TBP can prevent the defects on the surface of the coating and effectively improve the apparent performance of the material.

The gas-sealing coating was a dispersion of many different materials suspended in water and stabilized by surfactants. These surfactants can also stabilize foam, so some holes are observed in the samples without TBP (Fig. 6a). No large holes were observed in the samples with TBP (Fig. 6b), and the structure was uniform and dense, indicating that TBP can optimize the pore structure inside the materials, improve the density, effectively prevent the formation of large holes in the materials, and play the role of eliminating bubbles. It had been reported that TBP, a polar an odourless liquid, was highly efficient and

Table 1 The impact of TBP on air tightness

Items	Permeability coefficient (cm^3 cm m^{-2} s^{-1} $cmHg^{-1}$))	
	All cement samples	60% UFA + 40% cement samples
Without TBP	10.67×10^{-10}	3.84×10^{-10}
With TBP	5.68×10^{-10}	1.84×10^{-10}

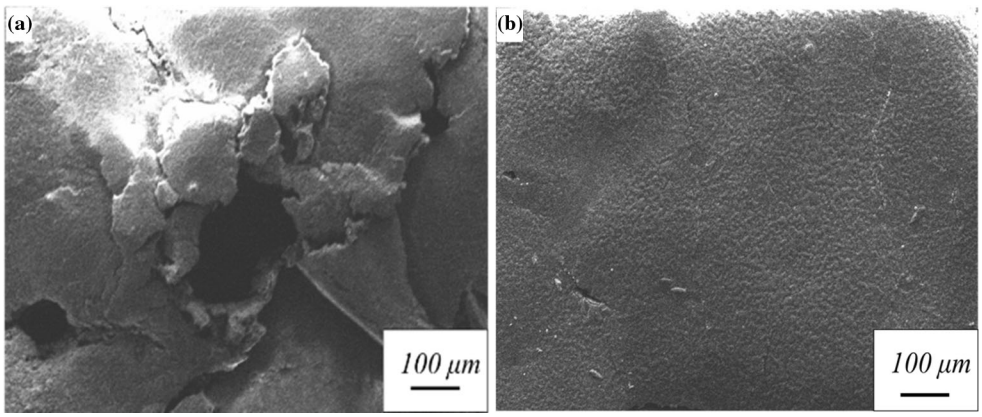

Figure 5 SEM images of the surface of containing 60% UFA samples (**a** without TBP; **b** with TBP).

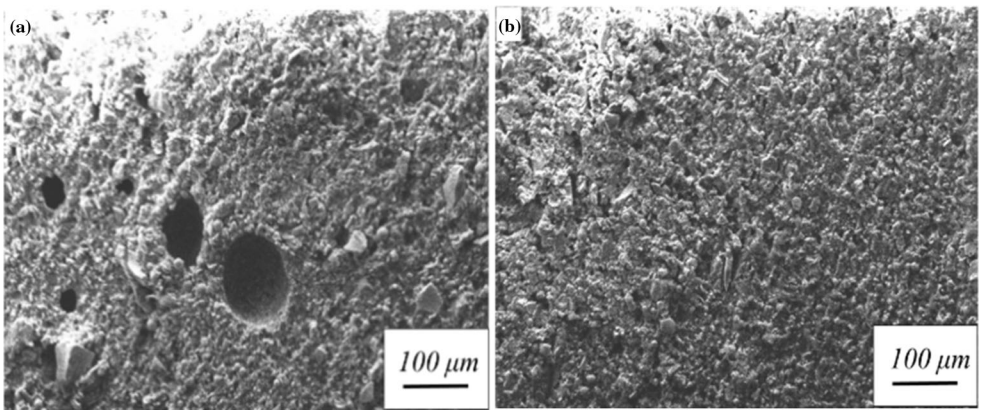

Figure 6 SEM images of the inner structure of containing 60% UFA samples (**a** without TBP; **b** with TBP).

suitable for use as an ideal antifoaming agent and as an adhesive in many industries [21, 22].

Effect and analysis of TBP on the combination effect of coating and coal samples

Effect of TBP on the penetration of coating in coal samples

In construction, the coating needs to not only be fully bonded with the coal wall after being sprayed on it, but it also needs to penetrate the coal seam to ensure its long-term gas-sealing effect [23, 24]. To investigate coating penetration, a spraying simulation experiment was performed in the laboratory. Two 500-ml empty reagent bottles with tops removed were employed. Then, the same amount of coal particles with the size of 1 mm to 5 mm (washed and dried) was added in the reagent bottles. The bottles were moderately shaken to make the inner structure of the coal samples compact and flat on the top. Up to 60 mL of coatings with and without TBP was placed in the bottles. After cultivation for 7 days, the reagent kits were cut axially. The coal particles, which were not bonded, were shaken off gently to obtain the coating permeability inside the coal samples, as shown in Fig. 7.

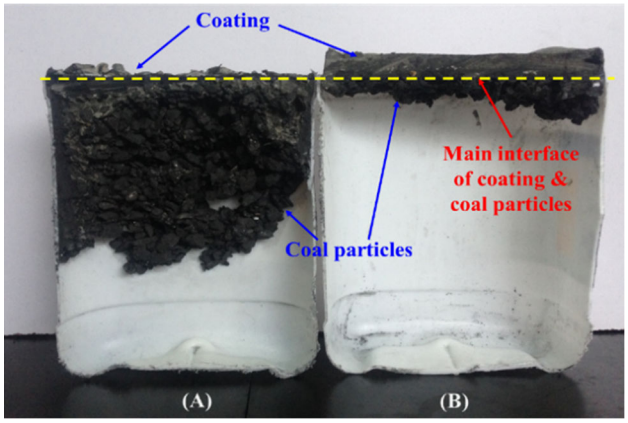

Figure 7 Penetration situation of different coatings in the coal samples (**a** with TBP; **b** without TBP).

For the samples without TBP, the penetration was not deep. Obviously, most of the coatings still accumulated on the external surface of the coal without achieving the effective penetration. In this case, the coating represented wasted material not good for the long-term application effect. The sample with TBP not only formed a layer of curing coating on the surface of the coal, but it also penetrated well into the coal system with many coal particles bonded and deeply penetrated. This was because TBP played a key role of fluidizing agent in the coating. It decreased the surface tension and viscosity of the coating, and then increased the fluidity of coating [25]. As such, the coating could penetrate deeply and promote the actual gas-sealing application of the coating on the roadway wall of the coal mine.

Effect of TBP on the microscopic combination and penetration of coatings

The coatings bonded with coal in Fig. 7a, b were selected for SEM analysis (Fig. 8) to observe the microscopic combination and penetration conditions with coal. Given that the coatings, which were smooth, can be made into the qualified samples for SEM test, the coatings in Fig. 8 are below and the coal particles are above.

In Fig. 8a, the coatings without TBP are mostly gathered at the contact interface between the coal sample and the material rather than penetrating from the interface to the internal coal particles. Only a small number of coal particles bonded on the surface of the contact surface are observed, and the coatings are poorly bonded with the coal particles with obvious gaps. Figure 8b clearly shows that the coatings with TBP bonded several coal particles. In addition, no blank space was basically observed at the bonding place. TBP enhanced the overall liquidity of the coating on the surface of coal particles and inside them. TBP promoted the coating to penetrate the coal and fill the holes between coal particles to make the internal structure of coal compact and improve the gas-sealing performance of the coating.

In order to investigate the coating properties, the main coating and interface coating in Fig. 8b were taken for FT-IR analysis. The main peak shapes of both samples in Fig. 9 are basically the same, indicating that their main components are the same. However, there are some differences in details. Both peaks of O–H and C=O in carboxyl group (–COOH) have weakened (http://www.science-and-fun.de/tools/). It might be the polycondensation reaction between –OH and some groups on the surface of coal. Although the exact explanation remains to be

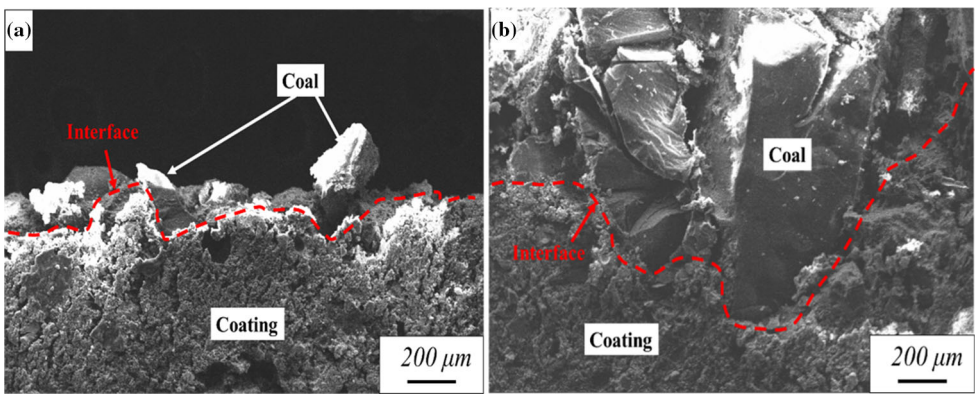

Figure 8 Photographs of the microscopic penetration and combination of different coatings in coal (**a** without TBP and **b** with TBP).

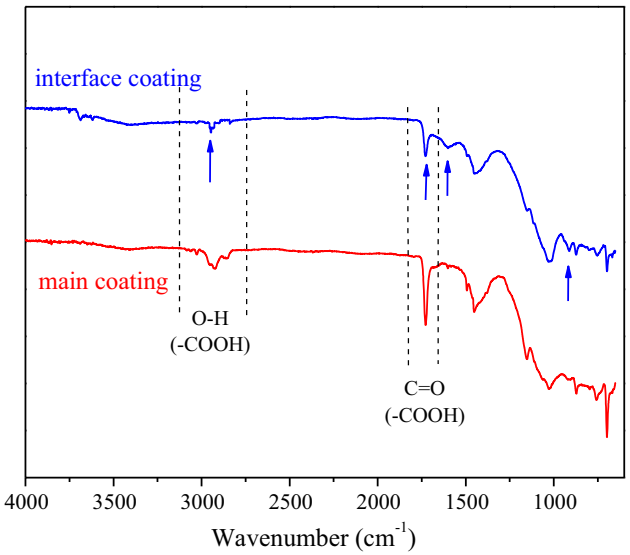

Figure 9 FT-IR spectra of main coating and interface coating.

studied, the existing experimental results show that interface coating can bond the coal particles well.

The effect analysis of TBP on the gas-sealing coating

TBP is hydrophobic oil (Fig. 10), and it could act as antifoamer and defoamer. The P(V) in TBP has strong complexation, which makes it easy to be adsorbed in the water–air surface. As such, the Marangoni effect was hindered, and the contact angle was decreased, which controlled the formation of foam. So in this way, TBP acted as a deaerating wetting agent. However, its low solubility in water made it form small droplets and be dispersible in the coating system and thus transport TBP droplets from bulk to the bubble interface (Fig. 11a). TBP had a low surface tension (27.79 mN m^{-1}, 20 °C), so it tended to flow towards the liquid forming foam with high surface tension. TBP particles could break through the activation barrier to push aside the surfactants, and then they could easily enter the air/water interface (Fig. 11b), which brings about dewetting at the same time. TBP particles constantly spread on the bubble surface (Fig. 11c), which made the local surface tension of the bubble decreased and led to a thinning film (Fig. 11d). Further, the bubbles exerted a strong drag on the underlying layers of water which causes the bubbles to ruptured subsequently (Fig. 11e) [26, 27].

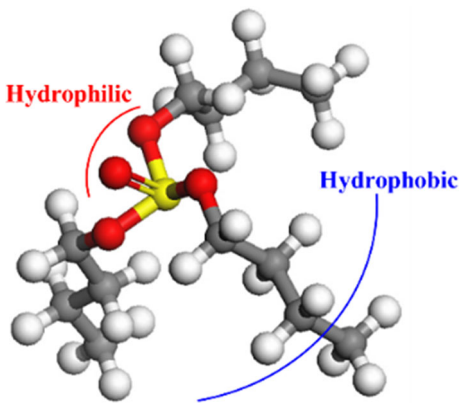

Figure 10 The structure of a single TBP molecule (yellow—P, red—O, grey—C, white—H).

Investigating the curing mechanism of the gas-sealing coating

Above experimental results indicated that during the curing of fly ash–cement-modified coating, a series of inorganic and organic chemical reactions may occur among water, emulsion, cement, and UFA in the raw material. It should be noted that functional additives were omitted in the study of this model.

1. Free Ca^{2+} of $Ca(OH)_2$ and calcium silicate hydrate (C–S–H) gel were produced after hydration of the cement. In styrene acrylic emulsion (SAE), many carboxyl groups, which can react with ionized calcium, were observed, and $[RCOO^-]Ca^{2+}[RCOO^-]$ and inorganic–organic compound gel were produced [28–30]. Possible interactions between these particles in this system are shown in Fig. 12.

First, a hydration reaction occurs in an alkaline environment.

$$C_{10}H_{11}COOH + OH^- \rightarrow C_{10}H_{11}COO^- + H_2O \quad (R1)$$

Second, the bridged linkage structure with Ca^{2+} can be formed after a reaction between the hydrated SAE and Ca^{2+} [31, 32]:

$$2C_{10}H_{11}COO^- + Ca^{2+} \rightarrow [C_{10}H_{11}COO^-]Ca^{2+}[C_{10}H_{11}COO^-] \quad (R2)$$

Figure 12 indicates that two carboxylate groups can be linked by one calcium ion. Two carboxylate groups from one SAE chain, such as in Fig. 12a, can be considered a self-link of the polymer chain. However, if two carboxylate groups belong to two SAE chains, two SAE chains should be chemically

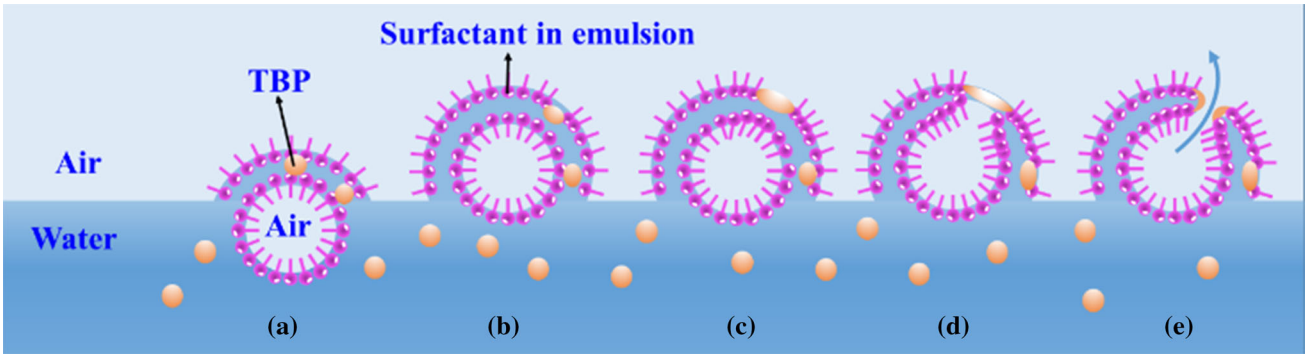

Figure 11 Defoaming mechanisms of TBP, **a** contacting, **b** entering, **c** spreading, **d** film thinning, **e** bubble rupture.

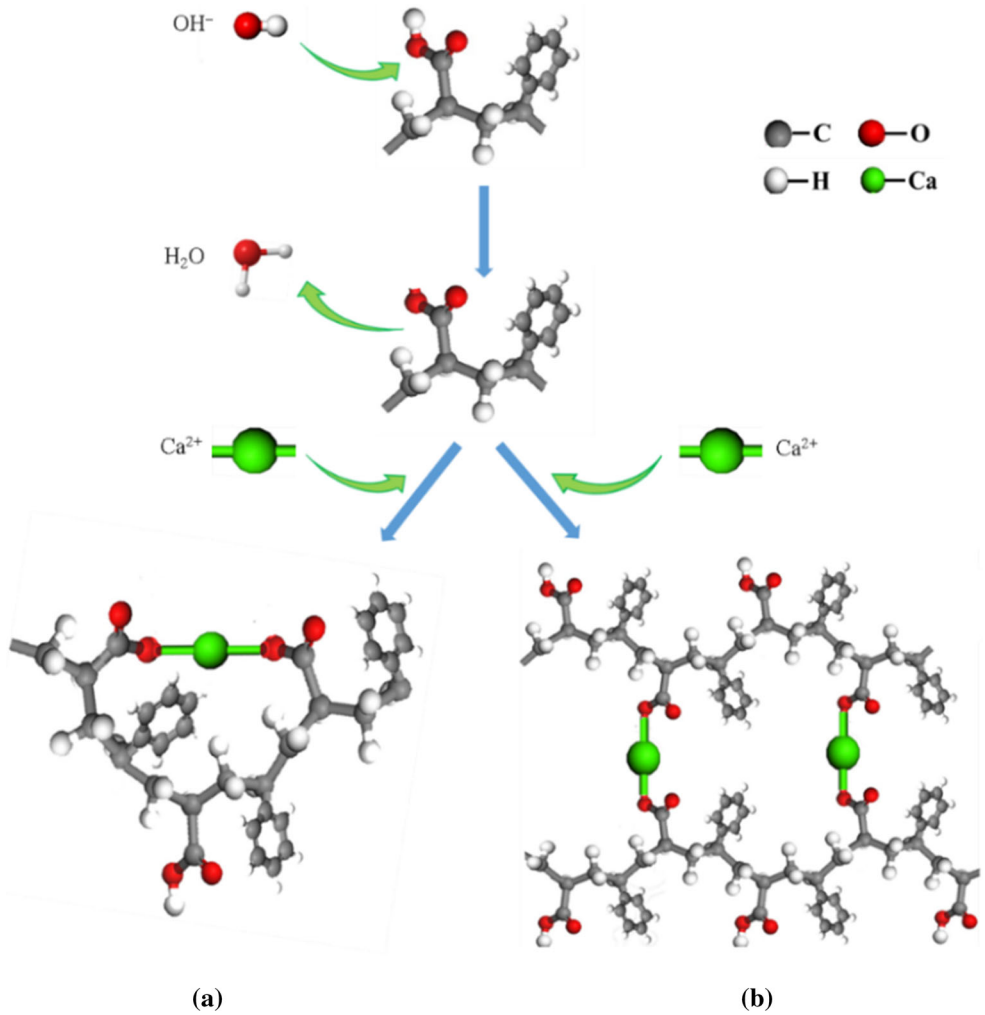

Figure 12 Schematic representation of Crosslinking reaction process between SAE and ionized calcium. **a** Self-link of polymer chain, **b** cross-link of plymer chains.

bonded together, which can be stated as a crosslink. As shown as in Fig. 12b, more crosslinks indicate strong bonding of two SAE chains [33, 34].

2. In addition, chemical interactions can also occur between SAE polymer chains and the activated groups of cement, fly ash or coal.

SAE polymer chain can react with C–S–H gel produced by cement hydration. Figure 13a is the schematic representation of the basic structural unit of the C–S–H phase, which is the layer of coordinated Ca sandwiched in between SiO_4 tetrahedral chains. The upper part shows an octamer silicate chain, whereas the lower part illustrates the incorporation of Al in a bridging site in the silicate chain structure [35]. Figure 13b is the schematic of polymer-modified C–S–H nanostructure.

The incorporation between SAE polymer chains and cement hydrate/cement grains also can be demonstrated as in Fig. 14. Thus, SAE particles can adhere firmly to cement grains/hydrates. As the concentration of calcium ions is relatively high around cement grains, the crosslinking between SAE chains would build a polymer network around cement hydrates [34]. As a result, the chemical bonding will enhance the attraction between SAE particles and cement hydrates/grains.

Many activated SiO_2 groups in fly ash can react with polymer chains through ionized calcium, and the crosslinked product bonded to the surface of UFA [39]. Figure 15 illustrates the polymer bonding to fly ash surface through the carboxylate group and the activated SiO_2 group. Additionally, coal possesses several activated –OH and –COOH groups on the surface. These groups would exhibit crosslinking reaction with the carboxylate group of polymer chain through ionized calcium. Then, the products bind to the surface of coal similar to that in Fig. 16. Similarly, these chemical bonding will enhance the attraction between SAE particles and UFA or coal.

Given the above findings, some chemical reactions may occur between the particle surfaces of SAE and, or cement, fly ash, and coal through calcium ions (Ca^{2+}) as illustrated in Figs. 14, 15 and 16. In addition, these reaction products formed the net structure accumulated on the surface of these solid particles. Such reactions are expected to improve the bond

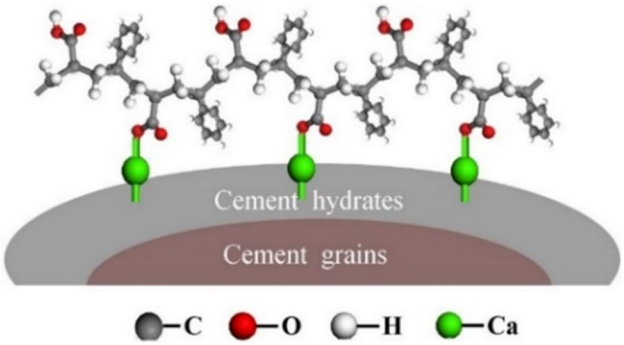

Figure 14 Schematic illustration of reaction between SAE and cement hydrates/grains.

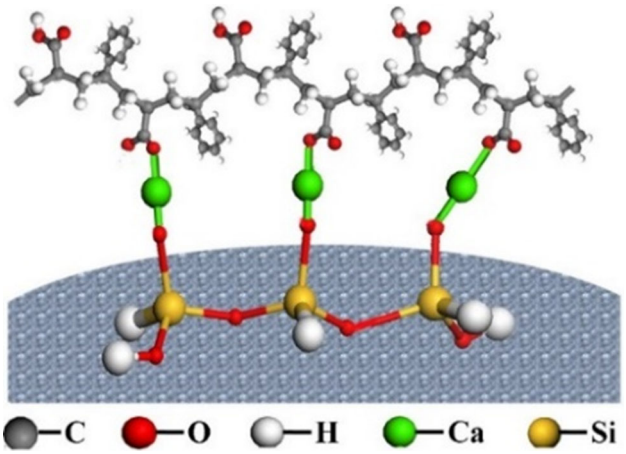

Figure 15 Schematic illustration of reaction between SAE and fly ash.

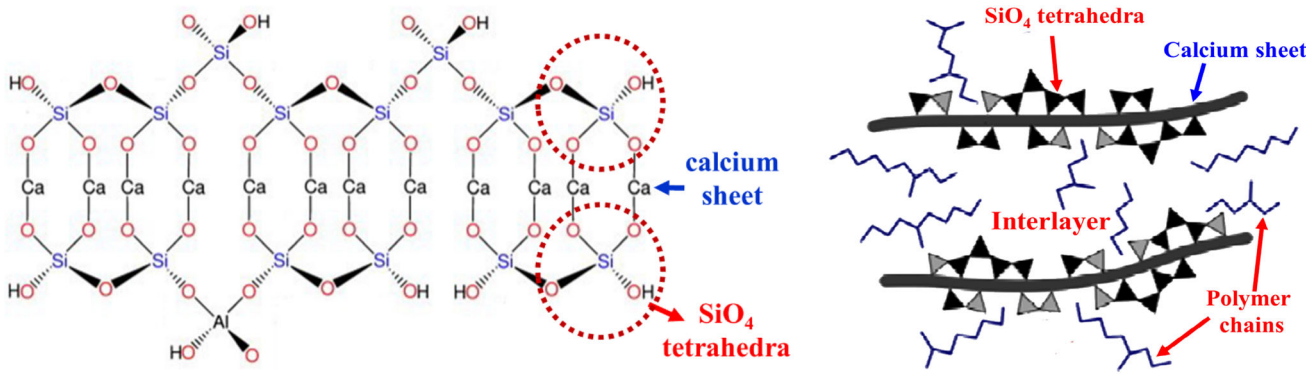

Figure 13 Schematic of **a** the basic C–S–H unit and **b** two simplified C–S–H modified by polymer [36–38].

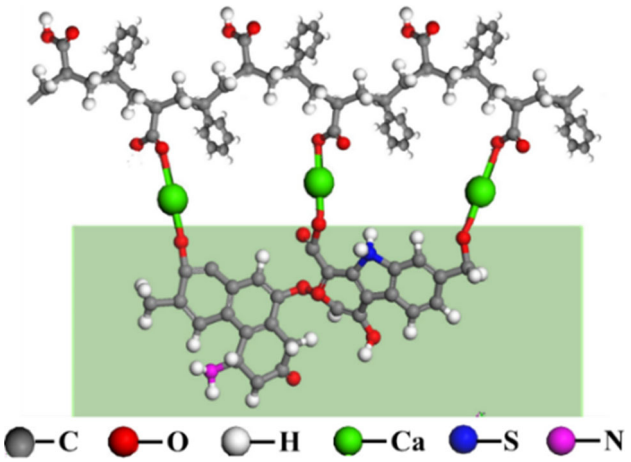

Figure 16 Schematic illustration of reaction between SAE and coal.

between polymer and solid particles and to improve the properties of sealing coating [39].

Some researchers mentioned that surfactant addition can further raise the solid–liquid ratio at the interface improving the interfacial bond by pore refinement and grain refinement. Gao et al. [40] reported that polyacrylate emulsion can react with cement hydrates and forms an interpenetrated network with large molecules composed by ion bond, therefore densifying the cement hydrates.

Model of the microstructure of the sealing coating and the composite mechanism

Sakai et al. [41] suggested a composite mechanism for the polymer-modified cement (PMC) mortar, wherein ethylene vinyl acetate and cement were the main materials. An improved four-step model was proposed to describe the forming of the microstructure of PMC mortar [42]. Considering the chemical reactions between cement hydrates and polymer latex, the corresponding influence of polymer latex on cement mortars was represented in the model. An improved model of the composite mechanism of SAE coating may be summarized as shown in Fig. 17.

1. After SAE was mixed with water, cement and fly ash, the mixtures were poured into coal particles. The spherical polymer particles independently distributed on the interface between solid particles due to their 'ball bearing' action of the polymer particles, the entrained air, and the dispersing effect of surfactants in the polymer latexes [39]. TBP adding also decreased the surface tension and viscosity of the coating, then increased the fluidity of the $[RCOO^{-}]Ca^{2+}[-RCOO^{-}]$ gel, and exhibited an excellent permeation into solid particles.
2. Then with hardening, the generated inorganic hydrates produced by cement and fly ash, and the organic product reacted between ionized calcium and polymer, fly ash, cement and coal. These products deposited and crowded around these solid particles. The large pores in the coating could be filled or sealed with these continuous reaction products. Additionally, a crosslinking film and membranes formed at the coating surfaces. Consequently, the adhesive property and crack resistance of the coating materials to coal increased, which provided a considerable increase in sealing property, including gas-sealing, water tightness, chemical resistance.

In order to partially validate the model, the FT-IR analysis was performed for the styrene-acrylic emulsion (polymer particle in Fig. 17a) and the coating after hardening shown in Fig. 18. There are obvious characteristic peaks of -COOH group in the infrared spectra of styrene-acrylic emulsion sample, while they are weakened in the coating after hardening. It might be the crosslinking reaction between SAE and other materials. But for the time being, there is no more accurate experimental verification. This will be our next important task.

Conclusions

Adding appropriate amount of surfactants in a coal-sealing coating can reduce its surface tension and improve the wettability with the contact interface. The efficacy of F202 and SD202 is affected by the emulsion concentration, while that of TBP is not affected obviously, and the contact angle reduction is always around 30–40%. These results indicate the strong modifying effect of TBP and its applicability. Specifically, TBP can reduce the defects of the coating surface and prevent the formation of large holes inside the coating to optimize its microstructure. Secondly, TBP effectively improves the wettability on the surface of the coal and makes the coating bond with the coal closely at the contact interface and penetrates deeply into the coal. Thirdly, TBP

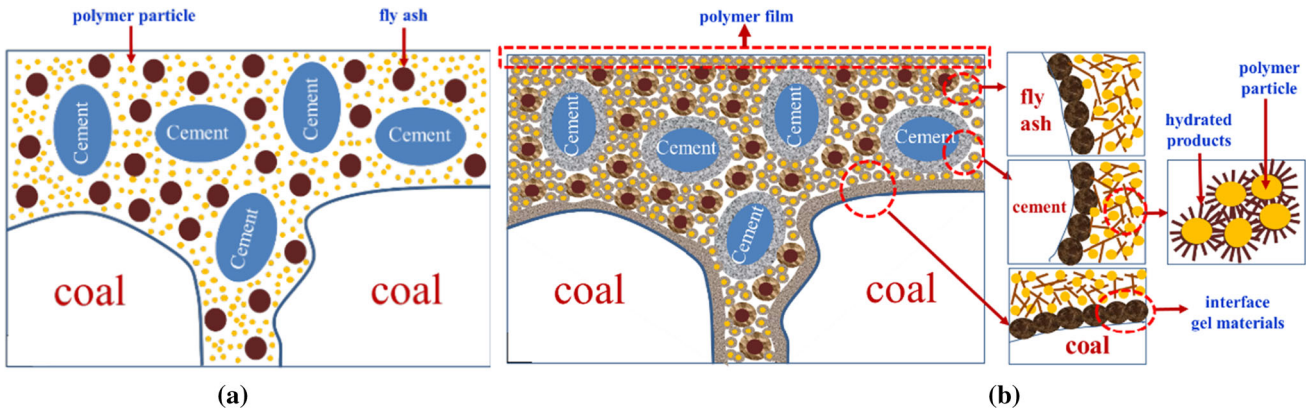

Figure 17 Schematic illustration of the composite mechanism model for sealing coating. (**a** before hardening; **b** after hardening).

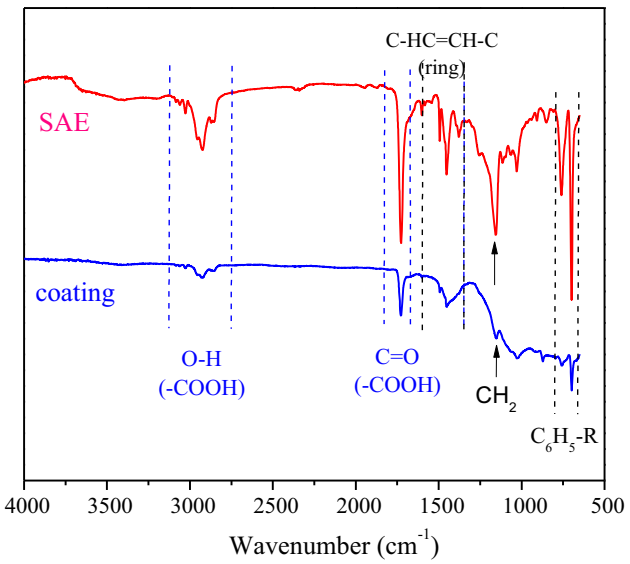

Figure 18 FT-IR spectra of SAE and coating after hardening.

obviously improves the liquidity of the inorganic–organic composite gel product and promotes the coating to penetrate the internal particles of coal and fill in the gaps between particles. As such, the gas flow resistance increases, and the permeability decreases sharply and reduces the gas emission strength and effectively improves the gas-sealing effect of the coating.

In this paper, an improved model for the composite mechanism of gas-sealing coating was proposed, but the verification for this model was not enough. In future, the NMR, SEM–EDS and other methods will be used to try to verify the gelation reaction and the bridge effect of the free Ca^{2+} in this model.

The sealing coating can be used in coal mine for improving the safety of underground mine workers. Fly ash as the main filler has a number of advantages including the reduction in the coating cost, solid waste utilization and protecting the environment.

Acknowledgements

This work was financially supported by the National Key Research Program of China (2017YFC0703104), the National Key Technology R&D Program (2013BAC14B05) and the Innovation Program of the Higher Education Institutions of Shanxi Province (2017106). Also, the authors would like to thank University of Wyoming for supporting this research.

Compliance with ethical standards

Conflicts of interest There are no conflicts to declare.

References

[1] Fu G, Cao JL, Wang XM (2017) Relationship analysis of causal factors in coal and gas outburst accidents based on the 24 model. Energy Proc 107:314–320. https://doi.org/10.1016/j.egypro.2016.12.160

[2] Fan CJ, Li S, Luo MK, Du WZ, Yang ZH (2017) Coal and gas outburst dynamic system. Int J Min Sci Technol 27:49–55. https://doi.org/10.1016/j.ijmst.2016.11.003

[3] Karacan CÖ, Ruiz FA, Cotè M, Phipps S (2011) Coal mine methane: a review of capture and utilization practices with benefits to mining safety and to greenhouse gas reduction. Int J Coal Geol 86:121–156. https://doi.org/10.1016/j.coal.2011.02.009

[4] Qin B, Lu Y (2013) Experimental research on inorganic solidified foam for sealing air leakage in coal mines. Int J

Min Sci Technol 23:151–155. https://doi.org/10.1016/j.ijmst.2013.03.006

[5] Zhai C, Hao Z, Lin B (2011) Research on a new composite sealing material of gas drainage borehole and its sealing performance. Proc Eng 26:1406–1416. https://doi.org/10.1016/j.proeng.2011.11.2318

[6] Han W, De XL, Han SS, Fu W (2015) Study on the wetting effect of water injection in coal seam. Safety 7:17–20. https://doi.org/10.3969/j.issn.1002-3631.2015.07.006 **(in Chinese)**

[7] Ma JY, Li C, Song HP, Cheng FQ (2013) The effect of fly ash on the performances of sealing material of coal seam gas. Fly Ash Compr Util 6:3–6. https://doi.org/10.3969/j.issn.1005-8249.2012.06.001 **(in Chinese)**

[8] Lin XY (2006) Additives for waterborne coatings. Paint Coat Ind 36:36–42. https://doi.org/10.3969/j.issn.0253-4312.2006.10.011 **(in Chinese)**

[9] Li Q, Lin B, Zhao S, Dai H (2013) Surface physical properties and its effects on the wetting behaviours of respirable coal mine dust. Powder Technol 233:137–145. https://doi.org/10.1016/j.powtec.2012.08.023

[10] Cheng WY, Pei JJ, Zhu K (2007) Study on reducing gas emissary of mine granules by surfactant. J North China Inst Sci Technol 10:1–5. https://doi.org/10.3969/j.issn.1672-7169.2007.04.001 **(in Chinese)**

[11] Denkov ND, Marinova KG, Tcholakova SS (2014) Mechanistic understanding of the modes of action of foam control agents. Adv Colloid Interface 206:57–67. https://doi.org/10.1016/j.cis.2013.08.004

[12] Saraf NM and Alat DV (2007) Bursting the bubble-foam killers. Int dyer 5:34–36. http://www.sarex.com/textile/wp-content/uploads/2015/08/231.pdf

[13] Song HP, Liu JQ, Xue FB, Cheng FQ (2016) The application of ultra-fine fly ash in the seal coating for the wall of underground coal mine. Adv Powder Technol 27:1645–1650. https://doi.org/10.1016/j.apt.2016.05.028

[14] Shubina V, Gaillet L, Ababou-Girard S (2015) The influence of biosurfactant adsorption on the physicochemical behavior of carbon steel surfaces using contact angle measurements and X-ray photoelectron spectroscopy. Appl Surf Sci 351:1174–1183. https://doi.org/10.1016/j.apsusc.2015.06.057

[15] Cipriano BH, Raghavan SR, McGuigan PM (2005) Surface tension and contact angle measurements of a hexadecyl imidazolium surfactant adsorbed on a clay surface. Colloids Surf A Physicochem Eng Aspects 262:8–13. https://doi.org/10.1016/j.colsurfa.2005.03.019

[16] Liu C, Li JH (2004) Handbook for application of surfactant, 3rd edn. Chemical Industry Press, Beijing (In Chinese)

[17] Lu F, Shi L, Yan H, Yang XJ, Zheng LQ (2014) Aggregation behavior of dodecyl triphenyl phosphonium bromide in aqueous solution: effect of aromatic ionic liquids. Colloids Surf A Physicochem Eng Aspects 457:203–211. https://doi.org/10.1016/j.colsurfa.2014.05.071

[18] Zhu K (2010) Experimental study on utilization of surfactants in reducing gas emission. Ph.D. Dissertation, China University of Geosciences **(in Chinese)**

[19] Zhu Y, Wu YK, Mao XY, Shi XJ, Liao YY (2015) Determination of solubility of tributyl phosphate in acid solution. J Kunming University Sci Technol (Nat Sci Ed) 40:1–4. https://doi.org/10.16112/j.cnki.53-1223/n.2015.01.001

[20] Zhou F, Shi B, Liu Y, Song X, Cheng J, Hu S (2013) Coating material of air sealing in coal mine: clay composite slurry (CCS). Appl Clay Sci 80–81:299–304. https://doi.org/10.1016/j.clay.2013.05.001

[21] Environment and Health Canada (2009) Screening assessment for the challenge: phosphoric acid tributyl ester (tributyl phosphate). Chemical Abstracts Service. Registry Number: 126-73-8

[22] Verschueren K (2001) Handbook of environmental data on organic chemicals, 4th edn. Wiley, New York

[23] Cheng Z, Xu Y, Ni GH, Li M, Hao ZY (2013) Microscopic properties and sealing performance of new gas drainage drilling sealing material. Int J Min Sci Technol 23:475–480. https://doi.org/10.1016/j.ijmst.2013.07.003

[24] Ni GH, Lin BQ, Zhai C. Li QG. Li XZ. Zheng CS (2013) Microscopic properties of drilling sealing materials and their influence on the sealing performance of boreholes. J University Sci Technol Beijing 35:572–579 (in Chinese). http://d.wanfangdata.com.cn/Periodical/bjkjdxxb201305003

[25] Li YM, Shi Y (2001) Study on the effect of tributyl phosphate on fluidity of GRC mortar. J Harbin Univ Sci Tech 6:13–14

[26] Chaisalee R, Soontravanich S, Yanumet N, Scamehorn JF (2003) Mechanism of antifoam behavior of solutions of nonionic surfactants above the cloud point. J Surfactants Deterg 6:345–351. https://doi.org/10.1007/s11743-003-0280-3

[27] Garrett PR, Ran L (2017) The effect of calcium on the foam behavior of aqueous sodium alkylbenzene sulphonate solutions. 3. The role of the oil in triglyceride-based antifoams. Colloid Surface A 513:415–421. https://doi.org/10.1016/j.colsurfa.2016.11.009

[28] Gao JM, Qian CX, Wang B, Morino K (2002) Experimental study on properties of polymer-modified cement mortars with silica fume. Cem Concr Res 32:41–45. https://doi.org/10.1016/S0008-8846(01)00626-3

[29] Larbi SZ, Bijen JA (1991) The interface between polymer-modified cement paste and aggregates. Cem Concr Res 21:983–990. https://doi.org/10.1016/0008-8846(91)90057-O

[30] Kang S, Kim J, Moon C, Song M (2015) Early hydration-retarding mechanism of polymer-modified cement. Mater Res Innovations 19:S8–S22. https://doi.org/10.1179/1432891715Z.0000000001610

[31] Bonapasta AA (2002) Cross-linking of poly (vinyl alcohol) chains by Ca ions in macro-defect-free cements. Chem Mater 14:1016–1022. https://doi.org/10.1021/cm010573q

[32] Wang R, Li J, Zhang T, Czarnecki L (2016) Chemical interaction between polymer and cement in polymer-cement concrete. Bull Pol Acad Tech 64:785–792. https://doi.org/10.1515/bpasts-2016-0087

[33] Mansur AAP, Santos DB, Mansur HS (2007) A microstructural approach to adherence mechanism of poly (vinyl alcohol) modified cement systems to ceramic tiles. Cem Concr Res 37:270–282. https://doi.org/10.1016/j.cemconres.2006.11.011

[34] Yang ZX, Shi XM, Creighton AT, Peterson MM (2009) Effect of styrene–butadiene rubber latex on the chloride permeability and microstructure of Portland cement mortar. Constr Build Mater 23:2283–2290. https://doi.org/10.1016/j.conbuildmat.2008.11.011

[35] Skibsted J, Hall C (2008) Characterization of cement minerals, cements and their reaction products at the atomic and nano scale. Cem Concr Res 38:205–225. https://doi.org/10.1016/j.cemconres.2007.09.010

[36] Raki L, Beaudoin J, Alizadeh R, Makar J, Sato T (2010) Cement and concrete nanoscience and nanotechnology. Materials 3:918–942. https://doi.org/10.3390/ma3020918

[37] Alizadeh A R (2009) Nanostructure and engineering properties of basic and modified calcium-silicate-hydrate systems. Ph.D. Dissertation, University of Ottawa, Canada http://dx.doi.org/10.13140/RG.2.1.3892.8089

[38] Beaudoin JJ, Raki L, Alizadeh R (2009) 29Si MAS NMR study of the modified C–S–H. Cem Concr Compos 31:585–590. https://doi.org/10.1016/j.cemconcomp.2008.11.004

[39] Ohama Y (1998) Polymer-based admixtures. Cem Concr Compos 20:189–212. https://doi.org/10.1016/S0958-9465(97)00065-6

[40] Gao JM, Morino K (2000) Research on polymer modified cement mortar containing silica fume. China Concr Cem Prod 5:8–10. https://doi.org/10.3969/j.issn.1000-4637.2000.05.003 **(in Chinese)**

[41] Sakai E, Sugita J (1995) Composite mechanism of polymer modified cement. Cem Concr Res 25:127–135. https://doi.org/10.1016/0008-8846(94)00120-N

[42] Beeldens A, Van Gemert D, Schorn H, Ohama Y, Czamecki L (2005) From microstructure to macrostructure: an integrated model of structure formation in polymer-modified concrete. Mater Struct 38:601–607. https://doi.org/10.1617/14215